Continuous Local Material Model for Cut Edge Effects in Soft Magnetic Materials

S. Elfgen, S. Steentjes, S. Böhmer, D. Franck, and K. Hameyer

Institute of Electrical Machines, RWTH Aachen University, Aachen 52062, Germany

Shape-giving production steps in the manufacturing of electrical machines often introduce plastic deformation and residual stress into the soft magnetic material, thus decreasing the magnetic quality and locally increasing both the static and dynamic hysteresis losses near the cut edges. Different models have been published, aiming to describe the changing local magnetization and loss behavior. Current approaches often consider permeability deteriorations by subdividing the soft magnetic material into the slices of different material properties. Three cut edge models are discussed here, where two describe the changed local polarization and the third estimates the resulting global iron losses. This paper presents a continuous material model for an efficient numerical model of the local magnetization. By replacing effortful sliced models, the continuous model is independent of the discretization and converges in the case of coarse meshes to the sliced model.

Index Terms— **Continuous material model, cutting edge, soft magnetic material.**

I. Introduction

DIFFERENT manufacturing techniques, such as laser cutting for prototyping or stamping during production, effect the local magnetic characteristics in a negative way and further differ considerably from their effects on the local resulting iron losses [1]. Depending on geometrical, material, and processing parameters along with the magnetic field strength, the iron losses resulting from different cutting techniques can differ by a factor of two or higher, due to increasing static and dynamic hysteresis losses [1]–[3]. Determining the local magnetic properties of soft magnetic materials used, for example, in electrical machinery, there is an essential part to consider the design and the finite-element (FE) simulations. The different cutting techniques introduce mechanical stress into the material, resulting in a locally decreasing permeability [4]–[6]. The influence of the cut surface gets more pronounced with the decreasing geometrical sizes leading to the superposing areas of degraded permeability [3], [4]. To cope with continuous, locally changing material properties, different models have been published describing local permeability distributions [7]–[9] or aiming at the resulting iron losses [10]. Current attempts approximate the different local material properties by subdividing the iron core of a model into slices [8], [9], [11]. The different material properties are homogeneous across the corresponding slices. The sliced approach is lacking due to the constant material properties inside the subdivision in accuracy. Moreover, the complicated modeling of slices arises during pre-processing. In light of these drawbacks, this paper compares different cut surface models and presents a continuous material model, established in the numerical FE simulation to describe the local distributed magnetic material properties. The model presented is based on the model published in [12]. This paper is structured as follows. Section II briefly explains the material characterization performed to identify the model parameters and compare the loss calculations with measurements. Section III compares and assesses three different models to consider the cut surface effects in the FE simulation. Section IV introduces the continuous material model, its implementation, and the results of FE simulations using this model. Hysteresis losses are calculated on the basis of the mentioned models and compared with the loss measurements described in Section II. Section V gives a brief discussion on the results along with an outlook for further studies.

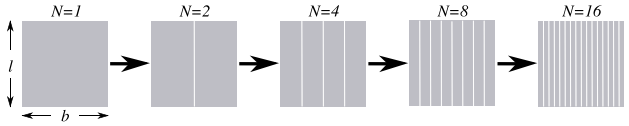

Fig. 1. Structure of single-sheet sample preparation.

II. Material Samples and Characterization

The required model parameters are identified using a set of single sheets of lamination. Starting with a basic sheet of 120 mm × 120 mm depicted in Fig. 1, samples with smaller width are consecutively cut out of the basic square. Thereby, single samples equaling a width b of 120, 60, 30, 15, 10, 5, and 4 mm are produced. The material used for the sample set is M330-35A, with Si = 2.9%, Al = 0.4%, P = 10 ppm, Mn = 0.13%, C = 29 ppm, S = 39 ppm, and an average grain size of 80 μm. It is cut by a CO_2 laser with a gas pressure of 10 bar, using a speed of 8 (m/min), a power of 1700 W, and a focus of a 5 in lens. The specimens are magnetically characterized according to the IEC standard 60404-4 using a single-sheet tester (SST), the field-metric method, and a quasi-static excitation. In order to compare the results of the FE simulations to a measurable geometry, five toroidal cores (TCs) are considered. The material and cutting parameters used are equal those of the measured single sheets. The yoke diameter sizes are 15 mm, 7.5, 5, 3.75, and 2.5 mm.

Manuscript received August 31, 2015; revised December 7, 2015; accepted December 21, 2015. Date of publication December 23, 2015; date of current version April 15, 2016. Corresponding author: S. Elfgen (e-mail: silas.elfgen@iem.rwth-aachen.de).

Color versions of one or more of the figures in this paper are available online at http://ieeexplore.ieee.org.

Digital Object Identifier 10.1109/TMAG.2015.2511451

III. Comparison of Different Models

A. Model 1

The first model, published in [13], is based on the conservation of energy. Derived therefrom, the model approach is defined, with the measured polarization J_{measured}, the strip width b, and the modeled local polarization distribution $\hat{J}_1(x)$. The local polarization distribution is defined by the experimentally verified, continuously differentiable function, using the distance from the center of the strip x, a material specific parameter A, and the maximum of the local polarization distribution $J_0(H)$ at a constant magnetic field H

$$J_{\text{measured}} = \frac{1}{b}\int_{\frac{-b}{2}}^{\frac{b}{2}} J_0 \frac{\cosh(A) - \cosh\left(A\frac{x}{x_0}\right)}{\cosh(A) - 1}\, dx. \tag{1}$$

The relationship between a measured polarization value and the modeled local distribution $\hat{J}_1(x)$ is achieved. This model provides a strip-width-dependent description of the local polarization and requires a constant field strength across the specimen. Three model parameters are defined, namely, parameters A, D the gradient at the cut edge $(d\hat{J}_1(x)/dx) = D$, and J_0. As the minimizing problem is not explicitly solvable, a boundary condition is set. In [13], the limit of the modeled local polarization is set to $J_0 \leq 1.1 \cdot J_{\text{measured}}$. The basis of the constraint is not explained further, but the deviation between the locally modeled and the measured polarization values rises with a higher magnetic field strength. To improve the modeled material characteristic, a new constraint is introduced limiting the maximum polarization of smaller strip width $J_0(b)$ by the undamaged specimen $J_0(b = 120\,\text{mm})$. The improved local polarization curves are shown in Fig. 2(a). Having a description of the local polarization, the local permeability can be calculated considering a constant field strength.

B. Model 2

The second model, published in [12], describes the local material behavior in terms of a locally dependent relative permeability. It involves three parameters, the permeability of an undamaged material sample $\mu_r(H, N = 0)$, the maximum permeability drop at the cut surface $\Delta\mu_{\text{cut}}(H)$, and the function $\eta(x)$ describing the local deterioration shape

$$\mu_r(H, x) = \mu_r(H, N = 0) - \Delta\mu_{\text{cut}}(H) \cdot \eta(x). \tag{2}$$

The parameter N equals the amount of cuts applied to a specimen. The local deterioration profile $\eta(x)$ generally depends on the cutting method used. In case of mechanical cutting, hyperbolic profiles are reported [4], [5], [13]. In the case of laser cutting, different profiles as well as non-symmetrical distributions are indicated in [14]. In the following, a parabolic permeability distribution is assumed described by $\eta(x)$:

$$\eta(x) = \begin{Bmatrix} 1 - \frac{x}{\delta} - a \cdot \frac{x}{\delta}\left(1 - \frac{x}{\delta}\right) & \forall & 0 \leq x \leq \delta \\ 0 & \forall & x > \delta \end{Bmatrix}. \tag{3}$$

The model parameter δ indicates the depth of the area influenced by the cut surface, while the parameter a is a compression factor. The maximum permeability drop at the cut surface $\Delta\mu_{\text{cut}}$ is defined in [12] as the difference between the permeability of the undamaged specimen and a damaged one. The expression should be constant for all the measured strip widths, which is achieved by scaling through a function value $F(N)$. The parameter identification is based on the single-sheet measurements mentioned in Section II. The resulting characteristic permeability curves are shown in Fig. 2(b), comparing the modeled permeability to the measurements of different strip widths. In view of the parameter identification of the resulting material characteristics, some adaptions have been made, which are described in Section IV.

C. Model 3

The third model, published in [10], correlates the total length of the cut l_{tot} of a specimen with the total mass m_{tot} and defines a cut surface factor S

$$S = \frac{l_{\text{tot}}}{m_{\text{tot}}} = \frac{2 \cdot N_s \cdot l}{m_{\text{tot}}} \quad \text{with} \quad m_{\text{tot}} = N_s \cdot l \cdot b_s \cdot d \cdot \rho. \tag{4}$$

The model aims on the resulting iron losses due to the influence of cut surfaces on the increasing proportion of the hysteresis losses. A linear description of the resulting losses is achieved. The model results considering the SST specimens at the quasi-static excitation are shown in Fig. 2(c). For different flux density values, a linear description can be used in order to estimate the resulting iron losses.

D. Comparison of the Models

The assessment of the three models is done in view of their applicability in the FE simulation, as the aim is a continuous, local material description considering the cut edge effects. All three models use SST measurements for model parameter identification. Models 1 and 2 assume a parabolic distribution of polarization, which is in accordance with other micromagnetic measurements [3], [14]. Model 1 comprises three major drawbacks in view of applicability on physical applications as an electric machine. First, the local material property depends on the strip width. Therefore, considering local material properties during FE calculations on an element basis requires determining the total material width surrounding every element. This leads to problems in areas without parallel boundaries. Second, to identify the local material properties in terms of permeability according to a defined strip width, it is necessary to previously know the expected polarization and the mean flux density across the area. This fact is the major drawback and clarifies the problems in terms of accuracy and applicability. Third, a constant magnetic flux across the specimen is assumed, which is inaccurate in the case of a toroidal core. In contrast, model 2 is a continuous material model describing the material properties in dependence on the distance to the cut edge. Therefore, it is possible to assign every element of an FE model a proper material characteristic depending on the magnetic field and the distance to the cut edge. Therefore, a consideration in the FE simulation is possible and will be presented in the following. Model 3 provides a scaling factor or a cut edge factor S using rising hysteresis losses along with a rising amount of cuts. Consequently, the model can only be used in postprocessing to scale the hysteresis losses. As shown in Fig. 2(c), the gradient

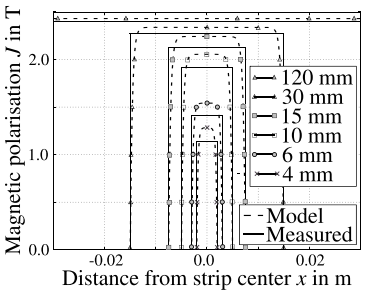

(a) Local polarisation $J(x)$ of model 1, limited by $J_0(b) \leq J_{\mathrm{measured}}(120\,\mathrm{mm})$.

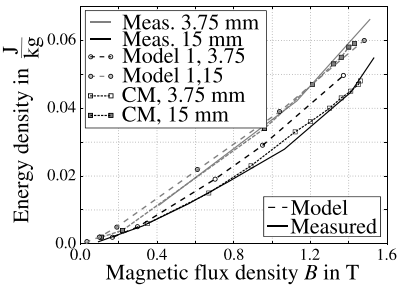

(b) Continuous material description of model 2.

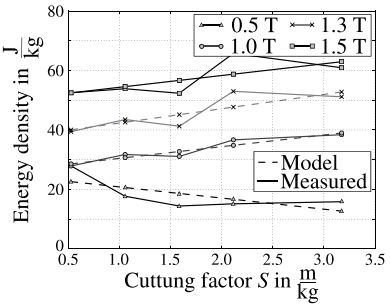

(c) Measured and calculated losses of toroidal cores using Model 3

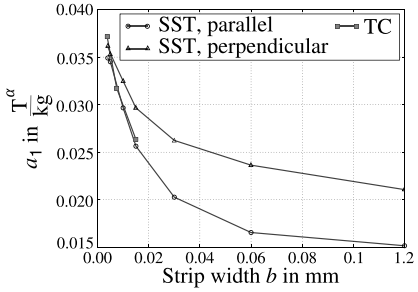

(d) Loss parameter $a_1(b)$

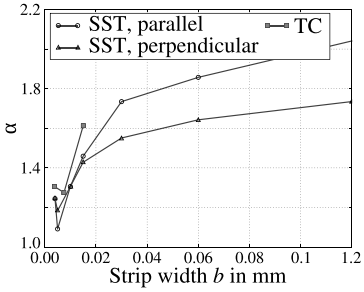

(e) Loss parameter $\alpha(b)$

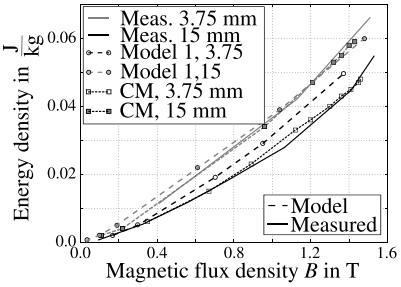

(f) Model 1 and the continuous model (CM).

Fig. 2. Results of the parameter identification considering (a) model 1 and (b) proposed CM. Furthermore, the identification of (d) and (e) hysteresis loss parameter dependent on the strip width and (f) resulting, calculated and measured iron loss, considering model 1 along with the proposed CM for exemplary TCs.

is depending on the mean flux density, and to estimate the resulting losses, at least two measuring points are required at a certain flux density for extrapolation. In summary, model 2 is currently the most suitable model to continuously describe the local material properties in the FE simulation and is considered in the following.

IV. Continuous Material Modeling in FE Simulation

To avoid the inaccuracies arising with sliced models in considering the cut edge effects [8], [9], [11], a continuous cut edge model based on model 2 is presented and used in the FE simulation. As mentioned, parameter identification is performed based on the single-sheet measurements of different strip widths. This study is carried out on laser cut specimens due manufacturing reasons; however, the proposed model offers the possibility of describing other cutting techniques as punched or shear cut specimen as well. In the process of parameter identification, accurate results are found when assuming parameter a to be constant $a = 1$. The local deterioration function $\eta(x)$ is limited by the quotient L/N, with L being the total width and N the number of cuts. The model does not cover a superposition of mechanical stress from both the cutting surfaces in the case of a small strip width $\delta > (b/2)$, which results partly in an overestimation of the local permeability, as shown in Fig. 2(b), and leading to an unsymmetrical polarization distribution. The interval boundaries are, therefore, replaced by $b/2$. In order to use the proposed continuous material model in the FE simulations, an algorithm assigning to each element a corresponding minimum distance to the cut surface is defined. The distance

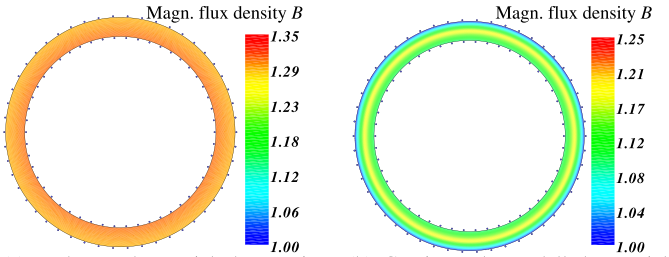

(a) Undamaged material characteristic.

(b) Continuously modelled material characteristic.

Fig. 3. Resulting flux density distribution of a toroidal core of 15 mm yoke width, using (a) characteristic material curve without cutting effects and (b) continuously modeled material behavior.

information is used as an additional property of the mesh element. A material matrix is assembled with a defined number of nonlinear material characteristics, which correspond to a particular distance to the cut surface. During simulation, material characteristics of an FE are assigned by interpolating the matrix entries according to the proper FE distance to the cut edge.

A. Iron Loss Calculations

In this section, loss calculations on the TCs are carried out, using models 1 and 2. As data basis for parameter identification, the single-sheet measurements are used. Hence, the TCs are simulated considering the local material characteristics shown in Fig. 3. The lower mean flux density across the yoke along with the magnetic field dependence of the cut edge effect can be observed. The resulting hysteresis losses are calculated according to [15] and compared with the measurement results.

With the identified hysteresis loss parameters a_1 and α from the SST measurements, the hysteresis losses are calculated considering the local flux density $B(x)$. The dependence on the strip width b is considered in the loss parameters a_1 and α, as shown in Fig. 2(d) and (e). The loss parameters are identified using the SST results. In addition, the matching loss parameters of different TCs are depicted. The hysteresis losses are calculated by integrating along the local flux density solutions $B(x)$ defined modeled on the soft magnetic area Ω

$$E_{\text{hyst}} = \int_{\Omega} a_1(b) \cdot B(x)^{\alpha(b)} d\Omega. \tag{5}$$

According to model 1, the strip width and the expected mean flux density are needed to derive the local permeability. Unaffected simulations are carried out to verify the needed field strength for a certain flux density and a strip width. The mentioned drawbacks in view of accuracy are obvious, as the expected mean flux density will be lower in a cut edge affected case. In the next step, parameter identification is carried out according to the assumed polarization and strip width. As the model does not provide magnetic field dependence and the local material characteristic is predefined by the model, only a single linear calculation step is performed. The resulting hysteresis losses of two TCs considering model 1 and the presented continuous model (CM) are depicted in Fig. 2(f). The calculated hysteresis losses of the proposed CM are in good agreement with the measured losses, whereas model 1 overestimates the losses in the case of the 15 mm toroidal core.

V. Conclusion

Three different approaches considering cut edge effects were compared in view of applicability in the FE simulation and its results in view of hysteresis loss calculations. Measured single-sheet specimens are used to identify the different model parameters. The advantages of the proposed CM that is only dependent on the distance to the cut edge are worked out. Hysteresis losses of TCs are simulated employing the different models. In the case of the CM, measured and modeled overall hysteresis losses of the TC areas are generally in good agreement. The applicability of the CM is applied to an exemplary stator geometry. In view of the continuous material description, two areas of further studies are necessary. With a rising amount of cuts, the permeability characteristic degenerates, leading to an overestimation of the local permeability. The maximum of the permeability curve shifts to higher field strength with a rising amount of cuts resulting in model inaccuracy, as the proposed model uses an exemplary permeability drop $\Delta\mu_{\text{cut}}$ to describe different material characteristics.

References

[1] S. Steentjes, G. von Pfingsten, and K. Hameyer, "An application-oriented approach for consideration of material degradation effects due to cutting on iron losses and magnetizability," *IEEE Trans. Magn.*, vol. 50, no. 11, Nov. 2014, Art. ID 7027804.

[2] A. Schoppa, J. Schneider, and C.-D. Wuppermann, "Influence of the manufacturing process on the magnetic properties of non-oriented electrical steels," *J. Magn. Magn. Mater.*, vols. 215–216, pp. 74–78, Jun. 2000.

[3] P. Baudouin, M. De Wulf, L. Kestens, and Y. Houbaert, "The effect of the guillotine clearance on the magnetic properties of electrical steels," *J. Magn. Magn. Mater.*, vol. 256, nos. 1–3, pp. 32–40, Jan. 2003.

[4] F. Ossart, E. Hug, O. Hubert, C. Buvat, and R. Billardon, "Effect of punching on electrical steels: Experimental and numerical coupled analysis," *IEEE Trans. Magn.*, vol. 36, no. 5, pp. 3137–3140, Sep. 2000.

[5] G. Loisos and A. J. Moses, "Effect of mechanical and Nd:YAG laser cutting on magnetic flux distribution near the cut edge of non-oriented steels," *J. Mater. Process. Technol.*, vol. 161, nos. 1–2, pp. 151–155, Apr. 2005.

[6] H. Naumoski, A. Maucher, L. Vandenbossche, S. Jacobs, U. Herr, and X. Chassang, "Magneto-optical and field-metric evaluation of the punching effect on magnetic properties of electrical steels with varying alloying content and grain size," in *Proc. 4th Int. Electr. Drives Prod. Conf. (EDPC)*, Sep./Oct. 2014, pp. 1–9.

[7] K. Fujisaki *et al.*, "Motor core iron loss analysis evaluating shrink fitting and stamping by finite-element method," *IEEE Trans. Magn.*, vol. 43, no. 5, pp. 1950–1954, May 2007.

[8] M. Bali, H. De Gersem, and A. Muetze, "Finite-element modeling of magnetic material degradation due to punching," *IEEE Trans. Magn.*, vol. 50, no. 2, Feb. 2014, Art. ID 7018404.

[9] L. Vandenbossche, S. Jacobs, X. Jannot, M. McClelland, J. Saint-Michel, and E. Attrazic, "Iron loss modelling which includes the impact of punching, applied to high-efficiency induction machines," in *Proc. 3rd Int. Electr. Drives Prod. Conf. (EDPC)*, Oct. 2013, pp. 1–10.

[10] B. Hribernik, "Influence of cutting strains on the magnetic anisotropy of fully processed silicon steel," *J. Magn. Magn. Mater.*, vol. 26, nos. 1–3, pp. 72–74, Mar. 1982.

[11] Z. Gmyrek and A. Cavagnino, "Analytical method for determining the damaged area width in magnetic materials due to punching process," in *Proc. 37th Annu. Conf. IEEE Ind. Electron. Soc. (IECON)*, Nov. 2011, pp. 1764–1769.

[12] L. Vandenbossche, S. Jacobs, F. Henrotte, and K. Hameyer, "Impact of cut edges in magnetization curves and iron losses in e-machines for automotive traction," in *Proc. 25th World Battery, Hybrid Fuel Cell Electr. Vehicle Symp. Exhibit. (EVS)*, Shenzhen, China, Nov. 2010, pp. 587–596.

[13] A. P. Schoppa, "Einfluss der be- und verarbeitung auf die magnetischen eigenschaften von schlussgeglühtem, nichtkornorientiertem elektroband," Ph.D. dissertation, Faculty Mech. Eng., RWTH Aachen Univ., Aachen, Germany, 2001.

[14] R. Siebert, J. Schneider, and E. Beyer, "Laser cutting and mechanical cutting of electrical steels and its effect on the magnetic properties," *Proc. IEEE*, vol. 50, no. 4, Apr. 2008, Art. ID 2001904.

[15] G. Bertotti, "General properties of power losses in soft ferromagnetic materials," *IEEE Trans. Magn.*, vol. 24, no. 1, pp. 621–630, Jan. 1988.